DECIPHERING SUBGLACIAL FROM TECTONIC DEFORMATION IN ANDRILL-1B

Senior Thesis

Submitted in partial fulfillment of the requirements for the

Bachelor of Science Degree

At The Ohio State University

By

Jessica Laine Greenberg

The Ohio State University

2019

Approved by

W. Ashley Griffith, Advisor
School of Earth Sciences

TABLE OF CONTENTS

ABSTRACT

The Victoria Land Basin (VLB) has undergone twelve glacial-interglacial cycles during the Late Pliocene. This region was susceptible to tectonic deformation from the half-graben in which the VLB is formed, as well as deformation due to glacial overriding. Furthermore, with the development of the Terror Rift the underlying sediment was further exposed to normal faulting. The samples used in this research were obtained from Andrill-1B located in the Windless Bight Region of the Terror Rift in the VLB. Through the microscopic analysis of thin sections and careful observation of core images between 152.12mbsf and 189.67mbsf I will determine whether the samples have undergone glacial deformation, tectonic deformation, or both.

ACKNOWLEDGEMENTS

I would first like to thank my two amazing research advisors Dr. Terry Wilson and Dr. Ashley Griffith.

I would like to express my immense gratitude to Dr. Terry Wilson for your guidance, mentorship, support, and patience with me during this long journey. I am extremely grateful to have had the opportunity to learn from you.

I am incredibly appreciative to Dr. Ashley Griffith for helping me complete this final piece for my degree.

My sincerest thanks to Dr. Anne Carey for always being so supportive, patient, and kind.

Scientific studies were supported by the US National Science Foundation cooperative agreement NSF-0342484 for ANDRILL.

Thank you to The Ohio State University, the School of Earth Sciences, and the Byrd Polar and Climate Research Center. You have given me the tools I needed in order to be successful, and the opportunity to explore my various interests in the field of earth science through coursework and research.

I would like to thank all of my wonderful classmates and my research group for helping make the geology department truly feel like home.

To my family and friends, thank you for your endless support and encouragement throughout this process.

Most importantly, I would like to express my deepest gratitude to my dad and my stepmom, Ellen. Thank you for believing in me, supporting me, and providing me with your unconditional love.

List of Figures

List of Tables

INTRODUCTION

The focus of this research is to decipher deformation due to glaciotectonism from that of tectonism in rocks of Late Pliocene age that were obtained from Andrill-1B sedimentary rock core, McMurdo Ice Shelf, Antarctica. Naish et al. (2007a) identified twelve glacial-interglacial cycles in the West Antarctic Ice Sheet (WAIS) and Ross Ice Sheet (RIS) during the Late Pliocene. The cycles are discernible by the alternations between diamictite (glacimarine and glacial) and diatomite (open marine) (Naish et al., 2007b).

During the glacimarine and glacial cycles, diamictites are unlithified and, therefore, may be subjected to deformation by the overriding glacier. A series of "Glacial Surface of Erosion" horizons have been identified throughout the AND-1B core, indicating where a grounded ice sheet is interpreted to over-ride the region. Sediment below these horizons may have undergone glacial deformation and may exhibit shear structures on the macro- and/or microscopic scale.

Andrill-1B (AND-1B) is situated within the Terror Rift and Victoria Land Basin (VLB), an area with known active tectonism during the Neogene. Tectonic faulting, specifically uppermost crustal brittle deformation, may therefore have affected the sedimentary sequence within the AND-1B core. The structures formed by the process will be macro- or microscopic.

The goal of this research is to determine the type(s) of deformation present within AND-1B sedimentary rocks and to attribute observed structures to either subglacial and/or tectonic processes. I examined six samples from between 150 to 190 meters below sea floor (mbsf). Through thin section and core analyses, I attempt to decipher features and/or structures that correspond to either brittle or ductile deformation. To aid in my identification and interpretation of the samples, I use documented examples of tectonic and subglacial structures, compiled from papers in the literature and, in particular, from Aber and Ber (2007).

BACKGROUND

Andrill-1B

Geologic Setting

The core used in this research is part of the McMurdo Ice Shelf (MIS) Project and was obtained in the Windless Bight region of the McMurdo Ice Shelf. In 2007, the MIS drill site was located in the northwest portion of the Ross Ice Shelf above the flexural moat basin that surrounds Ross Island. This area is part of the Victoria Land Basin (VLB), a half-graben that is ~350 km in length. The hinge of the half-graben is located along the Transantarctic Mountains (TAM) (Naish et al., 2007a, p. 121).

There has been significant rifting in the VLB since the late Eocene which has allowed approximately 10 km of sediment to accumulate. Furthermore, the drill site of AND-1B lies within the Terror Rift that formed within the VLB in the western Ross Sea. Extension within the VLB is associated with extrusive volcanism and alkalic igneous intrusions during the late Cenozoic. The result of this extension was the formation of the Terror Rift (Naish et al., 2007a).

Terror Rift is composed of high angle normal faults that trend in the north-south direction and dip to the east. The faults are bound along the East by intruded volcanic bodies that are arranged to form a line in the N-S direction with White Island forming the southernmost body. Naish et al. claim, "The volcanism is coeval with Late Miocene/Early Pliocene to recent extension in the Terror Rift and appears to be associated with a major west-dipping normal fault forming the east margin of a half graben that can be traced from Minna Bluff to Drygalski Ice Tongue" (Naish et al., 2007a, p. 125).

In addition to the faulting and volcanism, Naish et al. identified twelve glacial-interglacial cycles that occurred during the Late Pliocene. The authors use available age constraints for the strata to hypothesize that the twelve cycles occurred in less than a million years (Naish et al., 2007b).

Lithology of Samples

Krissek et al. (2007) identified eight lithostratigraphic units, which were divided in to twenty-five lithostratigraphic subunits (LSU), and eleven facies. The authors created graphical logs that provide substantial information, such as: the geologic age, unit, lithostratigraphic subdivisions, facies, depositional environment, the clay, silt, sand, and gravel content, and glacial proximity. Also, the depth is labeled along the left side of the graph in meters below sea floor (mbsf) (Krissek et al., 2007). Furthermore, the authors identified three additional facies, called motifs, that have been interpreted as representing different glacial regimes at the time of deposition. All of the samples in this research were deposited during Motif 2.

The samples used in this research were obtained from 152.12 mbsf, 166.64 mbsf, 167.60 mbsf, 168.00 mbsf, 178.04 mbsf, and 189.67 mbsf. The facies and LSU for each sample according to Krissek et al. (2007) are presented below and in **Table 1**.

Depth (mbsf)	Facies	Facies of Sample	Lithostratigraphic Subunit
152.12	4 ; 4 + 9	4	3.1
166.64	1a	1a	3.1
167.60	1a	1a	3.1
168.00	1a	1a	3.1
178.04	1a	1a	3.2
189.67	10	4	3.3

Table 1 – The facies and lithostratigraphic subunit (LSU) associated with the depth of each sample based on Krissek et al. classification.

Facies

1a – Diatomite

This is a weakly to massively stratified diatomite that is thinly laminated. The diatomite contains coarse sand, granules, and, occasionally, pebbles which are primarily volcanic in origin; however, intraclasts of diamictite and Transantarctic Mountain (TAM) lithologies are present. Also, lonestones are present within the diatomite and tend to be located "with sandy to granule-grade laminae/beds" (Krissek et al., 2007, p. 212). The lonestones may cause the underlying laminae to be deformed. Similarly, zones with extensive bioturbation may, also, deform the original stratification. Additionally, faulting is often present throughout this facies; however, faulting is "more intense" in the upper sections of the diatomite, especially in areas overlain by a diamictite.

The authors have subdivided Facies 1 into two categories: 1a and 1b. Krissek et al. (2007) state that, "Facies 1a consists of an almost pure diatomite lacking a significant terrigenous component, i.e. diatomite with lonestones and occasionally sandstone /gravel laminae or beds" (p. 212).

4 – Mudstone with Dispersed / Common Clasts

Krissek et al. (2007) observed Facies 4 to be composed of "silty claystones or mudstones with dispersed (< 1%) or common (1% - 5%) clasts" (p. 212). The clasts consist of several different lithologies and range in size from granules to small pebbles. This facies is often seen to grade in and out of stratified (Facies 9) and massive (Facies 10) diamictites. Consequently, mudstones containing clasts are commonly deciphered from Facies 9 and 10 by the lower abundance of sand (< 10%) in the matrix. Stratification may be present in the mudstone and, if so, is identified by changes in grain size along with change in color. Extensive bioturbation is possible, but for the most part is absent.

Similarly to Facies 1, the authors have divided Facies 4 into Facies 4a (stratified) and Facies 4b (subfacies) (Krissek et al., 2007). Unfortunately, I am unable to determine for my sample which of the two subfacies is present.

10 – Massive Diamictite

The compositional components and textural characteristics of this facies are nearly identical to that of Facies 9, except stratification is absent. The mud, clay, and sand content in the diamictite vary throughout the facies. Krissek et al. identified sharp lower contacts which are often attributed to load features. Also, the authors determined that Facies 10 can grade in or out or be interbedded with Facies 4 or 9. Fracturing is often observed throughout this facies (Krissek et al., 2007).

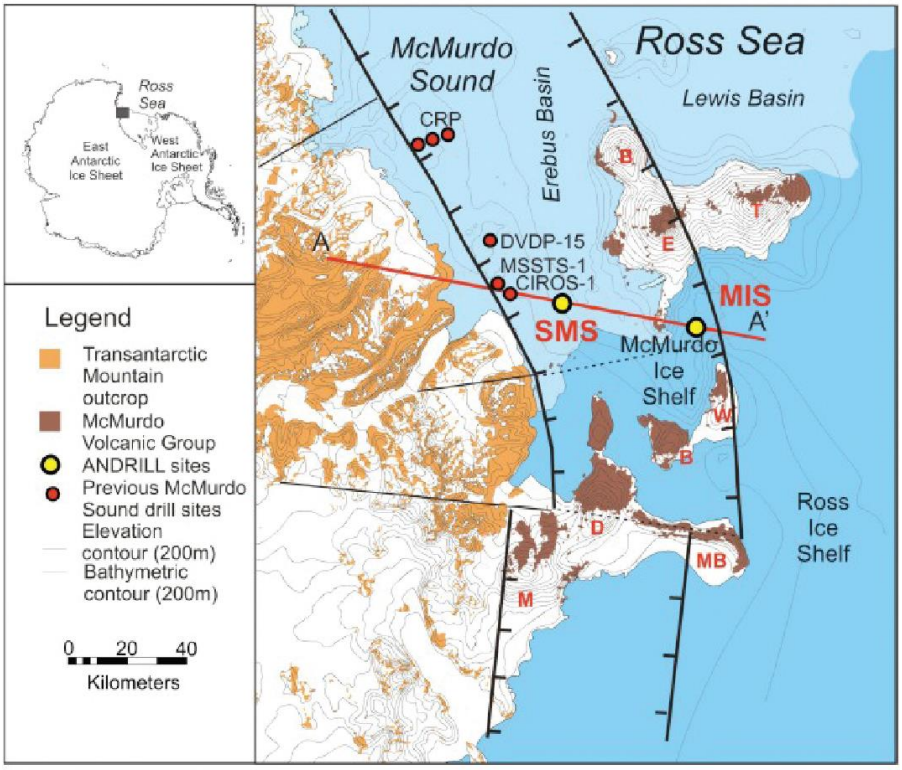

Figure 1 – The drill site for Andrill-1B is located at the yellow circle labeled MIS, at the eastern end of the cross section. The barbed lines represent the normal faults in the region with the barbs located along the hanging wall in the dip direction. The dashed lines indicate faults that have been inferred by the authors.

From (Naish et al., 2007a)

Figure 2 – Graphical log of sediments between 100 – 200 mbsf from AND-1B. The blue rectangle indicates the approximate range of depths used in this research.

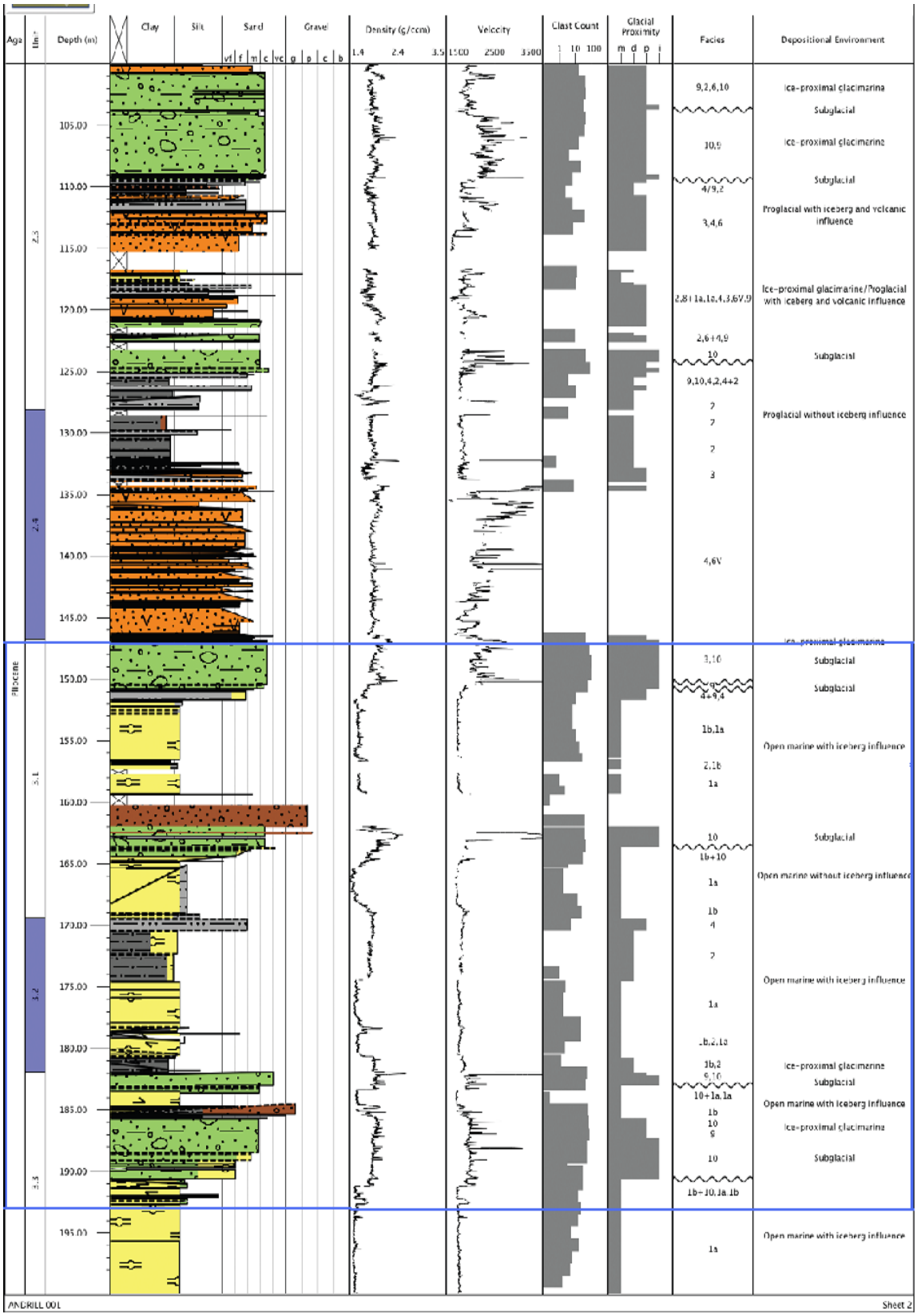

From (Krissek et al., 2007)

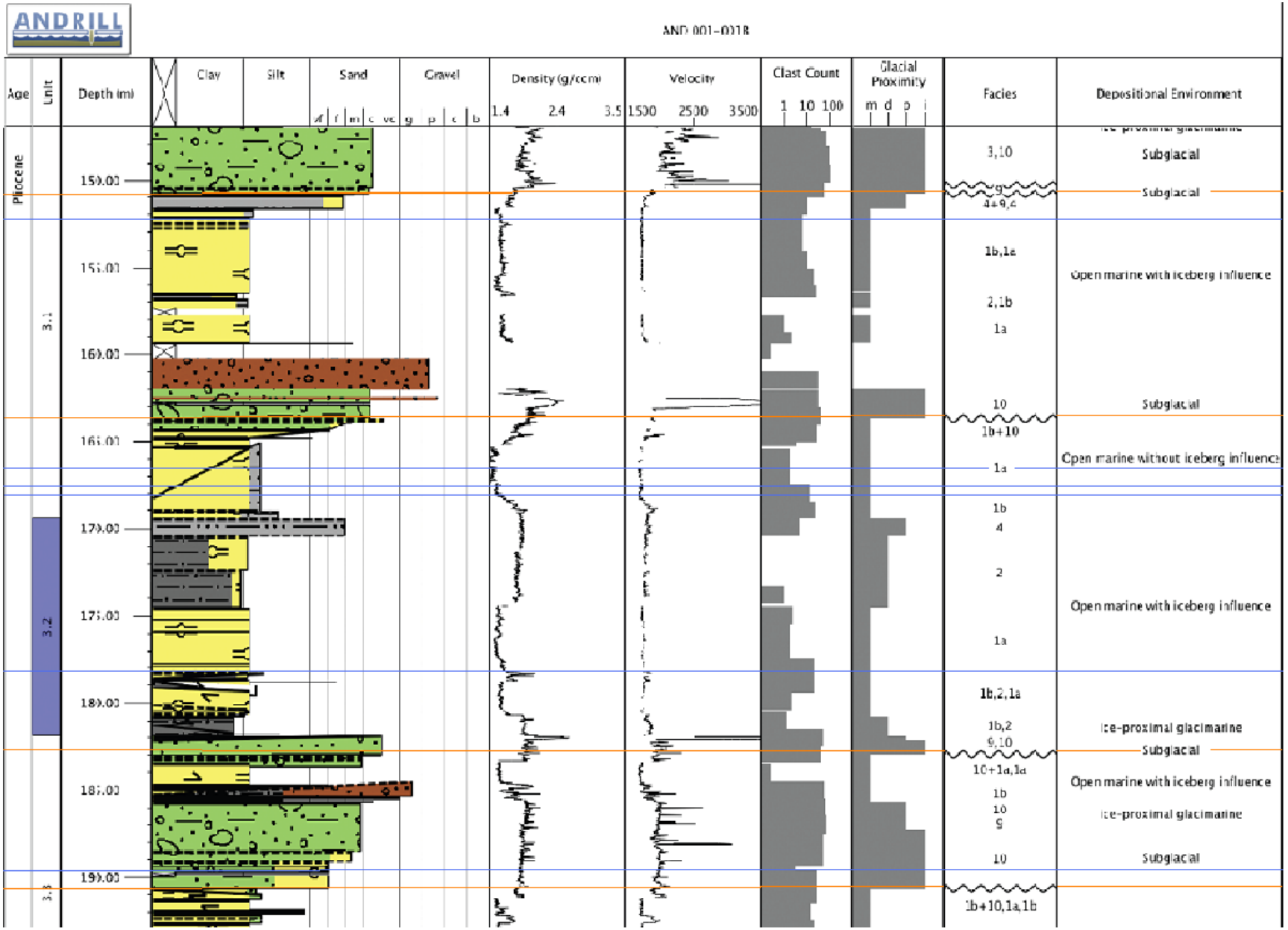
ANDRILL
AND-001-001B
Age
Unit
Depth (m)
Clay
Silt
Sand
Gravel
Density (g/cc m)
1.4
2.4
3.5
Velocity
1500
2500
3500
Clast Count
1
10
100
Glacial Proximity
Facies
Depositional Environment
Pliocene
3.1
3.2
150.00
151.00
160.00
161.00
170.00
171.00
180.00
181.00
190.00
3,10
Subglacial
Subglacial
1b,1a
Open marine with iceberg influence
2,1b
1a
10
Subglacial
1b+10
1a
Open marine without iceberg influence
1b
4
2
Open marine with iceberg influence
1a
1b,2,1a
1b,2
Ice-proximal glacimarine
Subglacial
10+1a,1a
Open marine with iceberg influence
1b
10
Ice-proximal glacimarine
Subglacial
1b+10,1a,1b

Figure 3 – Samples in the research are located between 152 – 190 mbsf. The lithostratigraphic units (LSU) are indicated beneath units. Under glacial proximity: i = ice contact; p = ice-proximal; d = ice-distal; m = marine. The wavy lines in the facies column represent glacial surface of erosion (GSE). The blue lines indicate the depths my samples were taken and the orange lines indicate the GSEs. Brown = conglomerate/breccia; green = diamictite; gray = terrigenous siltstone and sandstone; orange = volcanic sandstone, mudstone; pink = primary volcanic deposits; yellow = diatomite or biosiliceous-bearing mudstone (Naish et al., 2007b).

From (Krissek et al., 2007)

Lithostratigraphic Subunits

Subunit 3

Krissek et al. (2007) determined, "Lithostratigraphic Unit 3 still comprises a range of sediment types, but is distinguished on the basis of a change to biosiliceous- or diatom-bearing lithologies" (p. 203). Also, this unit has a noticeable change in lithology with the appearance of major alternations between diatomite and diamictite (Krissek et al., 2007).

3.1 – Clast-rich to Clast-poor Muddy Diamictite Alternating with Diatomite (146.79 to 169.40 mbsf)

The authors have identified LSU 3.1 to have two oscillations of diamictite/diatomite. The matrix consists of "fresh" volcanic glass along with a small amount of biosiliceous remains. Clasts range in size from granules to small pebbles and contain a variety of lithologies.

Due to a gap in the core between 159.34 to 160.19 mbsf, only one transition of diamictite to diatomite was able to be observed. This transition is noted as being gradual with an upward decrease in the mud content. However, the diatomite to diamictite transition is identified as being more abrupt with an upward increase in mud content. Krissek et al. (2007) claim, "this upper transition is characterized by physical mixing of the diamictite and diatomite lithologies via soft-sediment deformation and pervasive fracturing/faulting" (p. 204).

3.2 – Silty Claystone and Mudstone Alternating with Diatomite (169.40 to 181.93 mbsf)

LSU 3.2 primarily consists of continuous silty claystone and mudstone along with a few sections of diatomite. The top of this subunit is described as, a "greenish black mudstone with dispersed clasts" (Krissek et al., 2007, p. 204). The authors attribute the black color to the presence of pyrite. Unfortunately, as a result of the combination of soft-sediment deformation, pervasive fracturing/faulting, and bioturbation, any primary stratification has been obscured (Krissek et al., 2007).

The greenish black mudstone is conveyed as grading in the downward direction to an extremely dark gray silty claystone that is biosiliceous-bearing to biosiliceous-rich. Similarly to the mudstone, any notable primary stratification is obscured (Krissek et al., 2007).

At 174.50 mbsf, a sharp contact introduces the diatomite, which is present to 178.27 mbsf. Between 178.27 to 178.60 mbsf, the diatomite contains a diamictite constituent. This section is followed by a wedge of volcanic sandstone and biosiliceous-bearing silty claystone

that has been faulted and brecciated. The wedge is present from 178.60 to 178.73 mbsf. The top layer of diatomite has dispersed coarse sand, while the lower layer with diamictite includes sand clasts that range from granule to coarse which consist of metasedimentary and mafic volcanic clasts. Toward the bottom of the lower layer, the diatomite is described as becoming "silty clay bearing" (Krissek et al., 2007, p. 204). This change is terminated along an irregular sharp contact to a black silty claystone (Krissek et al., 2007).

3.3 – Alternating Diamictite and Diatomite (181.93 to 292.66 mbsf)

This lithostratigraphic subunit is composed of diamictite and diatomite beds that are continuously alternating. The diamictite beds range in thickness from 1.49 m. to 27.3 m and the diatomite beds range from 1.94 m. to 13.03 m. Krissek et al. identified five major diatomite/diamictite couplets. The upward transition of diatomite to diamictite is either gradational or abrupt, whereas the diamictite to diatomite transition is primarily gradational. Along the diatomite to diamictite boundary, either pervasive fracturing/faulting, soft-sediment deformation, or both have occurred. Conversely, the diamictite to diatomite boundary can be deformed or intact (Krissek et al., 2007).

The diamictite beds are mostly clast-poor, but contain a clast-rich layer along either the bottom or top of the bed. Clasts are angular to rounded in shape and are predominantly granule in size with small pebbles that arise locally. The clasts vary in composition, but the dominant composition is mafic volcanics. Within the diamictite are intermittent thin beds of sandy mudstone along with sparse beds of silty sandstone either with or without dispersed clasts. These intermittent beds are similar in lithology to the matrix of the diamictite. Also, biogenic carbonate is present sporadically throughout the diamictite in large (millimeter) sized fragments. According to the authors, there is a lack of primary layering within the diamictite which may be concealed as the result of soft-sediment and brittle deformation. Furthermore, areas that have undergone extensive deformation may simulate the appearance of a breccia (Krissek et al., 2007).

Diatomites in this subunit consist of varying abundances of sand along with occasional granules and pebbles. Grains are typically dispersed; however, when located in close proximity the grains become concentrated and form lenses. The lenses range in thickness from a single grain to a centimeter. There are yellow laminae that appear sporadically in the diatomites. Fracturing and/or faulting are present which may be sufficiently pervasive to brecciate the rock (Krissek et al., 2007).

Naish et al. claim that diamictites are characteristic of glacial and glacimarine settings while diatomites represent open marine settings. Furthermore, the authors describe the basal contact of diamictites along with the top few meters of diatomites as being glacially sheared and deformed (Naish et al., 2007b).

Motif

Krissek et al. identified three facies successions that have been interpreted as depositional records of the sediment under clearly different glacial regimes. Motif 2 occurs between ~ 82.7 mbsf – 586.59 mbsf and is dominated by interstratified diamictite and diatomite. The authors were able to recognize an upward trending sequence of lithologies that are interpreted as a glacial retreat followed by an advancement of ice (Krissek et al., 2007).

Glacial retreats are interpreted as consisting of a glacial surface of erosion (glacial maxima) followed by a massive diamictite, stratified diamictite or mudstone, sandstone,

interstratified sandstone and mudstone, mudstone, and then diatomite (glacial minima/marine). Periods of ice advancement are interpreted to consist of a mudstone, sandstone and mudstone, rhythmically stratified sandstone and mudstone, or conglomerate, followed by a stratified diamictite that is immediately below a glacial surface of erosion (glacial maxima).

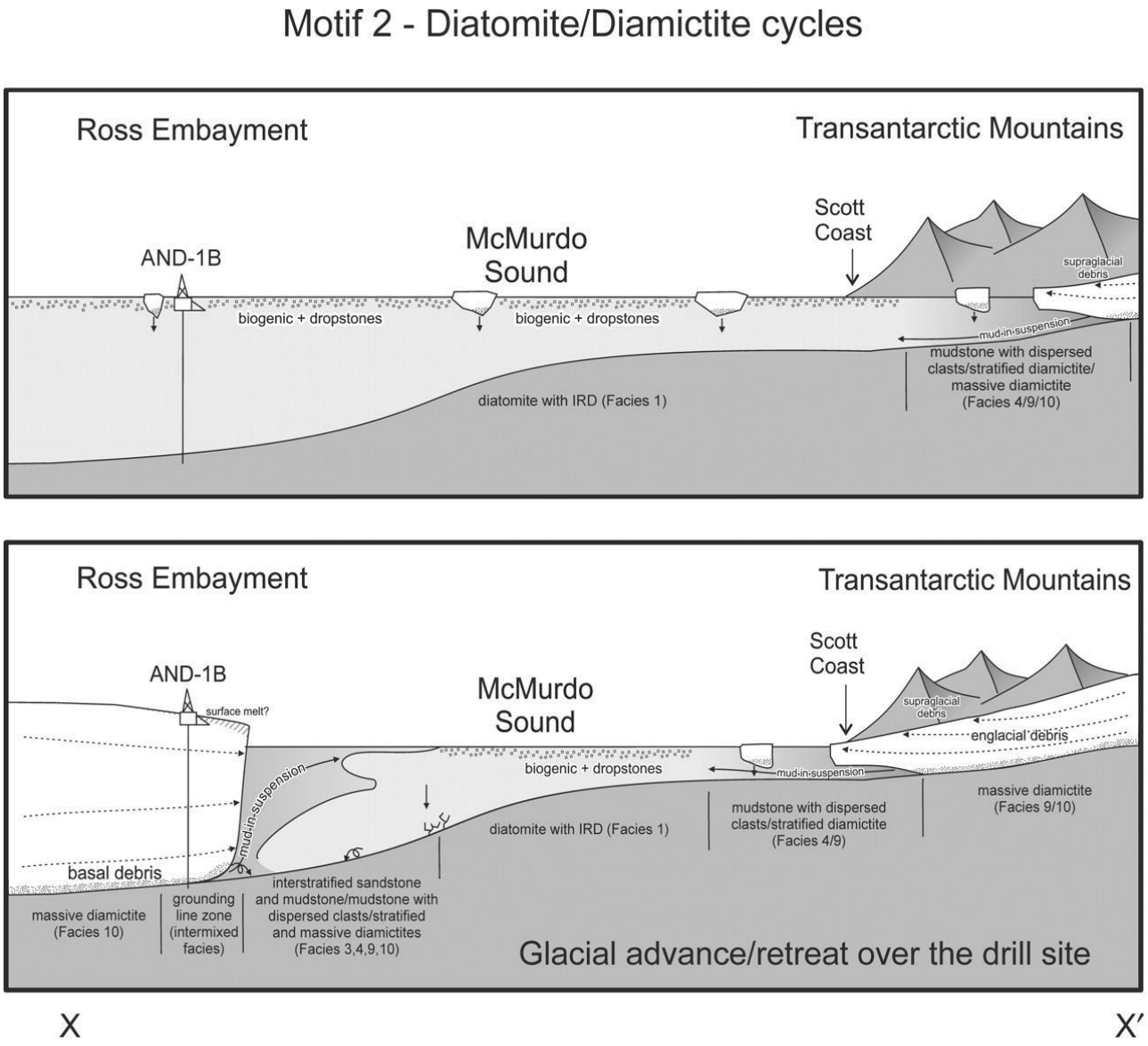

Figure 4 – The images illustrate the facies present in cross-section between ANDRILL-1B and the Scott Coast during a glacial retreat, or marine setting, (top) and an ice-sheet advancement (bottom)

From (McKay et al., 2009)

Glacial Surface of Erosion

A "Glacial Surface of Erosion" (GSE) is an area within the sediment that has been

identified as the top of a subglacial shear zone. GSEs are uncomfortities within the sediments that have been interpreted as being in contact with the overriding ice-sheet (**Figure 2**). In AND-1B, GSEs primarily occur beneath massive and stratified diamictites that overlie deformed or brecciated marine or glacimarine lithofacies. The diamictite overlying the contact is intermixed with the underlying facies and grades upward into a massive diamictite. McKay et al. claim, "this is interpreted to be the result of homogenization by subglacial shearing" (McKay et al., 2009, p. 1543). Also, the GSE commonly contains clastic intrusions and exhibits high levels of shearing. The authors assert that these contacts are consistent with recognized examples of sediments that have been subglacially deposited and overrode by grounded ice. The diamictite and other sediments above the contact are interpreted as glacial advances and maximums followed by retreat of grounded ice. The glacimarine sediments are interpreted as developments of the ice sheet and marine sediments as glacial minimums (McKay et al., 2009).

There are 58 unconformities within AND-1B that have been interpreted as GSEs. Four GSEs are present between 150.00 to 191.00 mbsf. GSEs occur at: 150.73 mbsf, 163.65 mbsf, 182.99 mbsf, and 190.63 mbsf (McKay et al., 2009). The subglacial shear zone extends between 5 to 10 m below the grounded ice (Wilson et al., 2008). The samples used in this research were selected specifically to look for subglacial deformation based on the samples' proximity to a GSE. The vertical distance between the samples and the closest GSE are shown in **Table 2**.

Sample	GSE	Meters Below GSE	GSE	Meters Above GSE
152.12 mbsf	150.73 mbsf	1.39 m	163.65 mbsf	11.53 m
166.64 mbsf	163.65 mbsf	2.99 m	182.99 mbsf	16.35 m
167.60 mbsf	163.65 mbsf	3.95 m	182.99 mbsf	15.39 m
168.00 mbsf	163.65 mbsf	4.35 m	182.99 mbsf	14.99 m
178.04 mbsf	163.65 mbsf	14.39 m	182.99 mbsf	4.95 m
189.67 mbsf	182.99 mbsf	6.68 m	190.63 mbsf	0.96 m

Table 2 – The vertical distances between four identified glacial surface of erosion (GSE) and the samples. In the "Meters Below GSE" column, the depths highlighted in red are within 10 m below the GSE and may be in the shear zone. In the "Meters Above GSE" column, the depth highlighted in red is within five meters of the GSE and may represent sediment that has been intermixed with diamictite through glacial homogenization.

Samples 152.12 mbsf, 166.64 mbsf, 167.60 mbsf, and 168.00 mbsf are all within 5 m below an identified GSE. It is very likely that these samples have undergone deformation due to an overriding glacier or ice sheet. Samples 166.64 mbsf, 167.60 mbsf, and 168.00 mbsf are all Facies 1 diatomites which is consistent with the marine or glacimarine sediment found to occur below GSEs by McKay et al. Samples 189.67 mbsf is within 10 m below an identified GSE and, therefore, may have structures formed by subglacial deformation. Also, samples 152.12 mbsf and 189.67 mbsf are Facies 4 which may be present with Facies 10 (no bioturbation or clasts), with Facies 10 and dispersed/common clasts (no bioturbation), or with dispersed / common clasts and bioturbation (no Facies 10). Sediments that are present with Facies 10, but lack bioturbation and clasts may indicate subglacial deposition. Sediments with Facies 10 and clasts and without

bioturbation indicate deposition beneath iceberg zones. Sediments with bioturbation indicate a marine setting; clasts may be present due to floating ice. Sample 189.67 mbsf is only ~ 1 m above a GSE. This facies may be present above the GSE due to glacial homogenization and intermixed with a diamictite. Furthermore, all of the samples, except 178.04 mbsf, may display shearing/deformation from an overriding glacier (McKay et al., 2009).

Natural Fractures Observed by Core Logging

Wilson et al. deciphered 1,475 natural fractures in AND-1B. Natural fractures are defined as, "pre-existing fractures in the rock that are intersected by coring" (Wilson et al., 2007, p. 4). These fractures are identified based on geometry and features such as brecciation (Wilson et al., 2007).

The authors observed there to be a high volume of fractures between 125 – 300mbsf. Wilson et al. describe faults with "surface kinematic indicators" as the result of normal-sense faulting. Although, a subset of faults displaying reverse-sense displacement were identified in close proximity to the normal-sense faults. The presence of the reverse-sense faults is possibly the result of the sediment undergoing glacial overriding. Also, due to the structural nature of rift basins there are conjugate faults present (Wilson et al., 2007).

Kinematics and Deformation

Glaciotectonic Deformation

Aber and Ber define glaciotectonism as, "glacially induced structural deformation of bedrock or sediment masses as a direct result of glacier-ice movement or loading" (Aber and Ber, 2007). Glacial (or ice-sheet) deformation is the result of dynamic (forward) movement or static (vertical) loading. Often, both processes occur simultaneously (Aber and Ber, 2007).

In 1973, Occhietti devised a list of five categories in which glacial deformation may occur. Only three of the categories are relevant to this research, which are: glaciotectonic, glaciodynamic, and glaciostatic.

- Glaciotectonic – Pre-existing substratum (i.e. bedrock) that is deformed by active overriding ice movement.
- Glaciodynamic – Ground moraine undergoing active ice movement which produces primary structures.
- Glaciostatic – The deformation of substratum and ground moraine from static ice-loading.

(Aber and Ber, 2007)

There are two fundamental criteria used in identifying glaciotectonic structures and landforms:

1. The presence of recognizable pre-existing sediment bodies or bedrock

and

2. Within these bodies, the presence of glacially induced structures.

Based on the type of deformation present, glaciotectonic structures can be divided into two categories – ductile and brittle. Ductile deformation resembles the flow or internal creep behavior of a fluid or plastic. A rock mass undergoing ductile deformation, essentially, has no internal strength. This allows for minute changes in pressure to result in substantial changes in the size and shape of the rock mass. The types of rocks that typically exhibit ductile structures are unconsolidated or fine-grained strata (i.e. chalk, clay, shale, or silt) that are subjected to high confining pressures. Brittle deformation is identified by fractures that form by failure along discrete planes within a rock mass. Rocks that undergo brittle deformation are moved or adjusted along fault planes with no permanent deformation to the internal fabric of rocks between fractures. The types of rocks that typically exhibit brittle structures are coarse-grained or consolidated strata (i.e. gravel, sand, sandstone, limestone, or quartzite) that are subjected to low confining pressures. A few examples of brittle structures that display brittle deformation are faults, breccia, joints, and fissures. Often, brittle and ductile deformation are associated within the same sequence of deformed strata. As the thickness and lithology change within a stratified sequence so does the response to deforming pressure (Aber and Ber, 2007).

Macroscopic Structures

Glaciotectonic macroscopic structures are essentially the same as those created by tectonic deformation (i.e. folds, faults, and fractures). In order to decipher glacial from tectonic deformation, geometric and kinematic analysis should be used. Geometric analysis relies on descriptive/structural analysis and terrain analysis. Structural analysis attempts to determine: the geometry of the structure, age of structure, and genesis of the structure. Terrain analysis relies upon landscape topography, vegetation, drainage, and soils to reflect the nature of subsurface structures. Kinematic analysis measures the strain(s) within a rock mass and then uses the strain to understand the stress field from which the strain was induced (Aber and Ber, 2007).

It is reasonable to believe that the glacial deformation in the samples will be ductile/shear. Most likely, at the time of deformation the rocks were not fully lithified allowing shearing to occur. Also, while being over-rode by a glacier, water was present in the rocks which enabled ductile deformation to occur.

The macroscopic structures that could be observed are mineral lineation, σ-type structures, δ-type structures, fractured grains, veins, boudins, folds, and/or faulting.

Microstructures

van der Meer et al. (2003) identified several microfabrics and microstructures associated with glaciotectonics (**Figure 6**). A few microstructures that van der Meer et al. do not mention are δ-type complexes and σ-type complexes. These structures form by shearing and indicate shear-sense (van der Pluijm and Marshak, 2004).

Tectonic Deformation

Macroscopic Structures

The samples observed are within 200 mbsf which has very low temperatures and low pressures. As a result of tectonism, these conditions allow only brittle deformation to occur. The tectonic deformation expected for the samples in this research are conjugate sets of normal faults

with dips of ~ 60°. As previously mentioned in the geologic setting, AND-1B is from the VLB, a half-graben. A half-graben is defined as having one border that is a normal fault (van der Pluijm and Marshak, 2004). Also, AND-1B is in the Terror Rift which has undergone extensional deformation. Consequently, the deformation could have occurred after the rocks were lithified or while the sedimentary rocks were unlithified. The cores may exhibit fractures, veins, slickensided surfaces, striae, or dark millimeter sized bands that are probably slickensided faults (Wilson et al., 2007).

Microstructures and microfabrics

The microstructures expected are nearly identical to the macroscopic structures. The structures expected are conjugate normal faults, fractures, conjugate normal microfractures, veins, or soft-sediment deformation.

Microfabrics are plasmic fabrics that may be indicative of ductile, brittle, ductile/brittle, or pore-water induced deformation to the rock (Menzies, 2000).

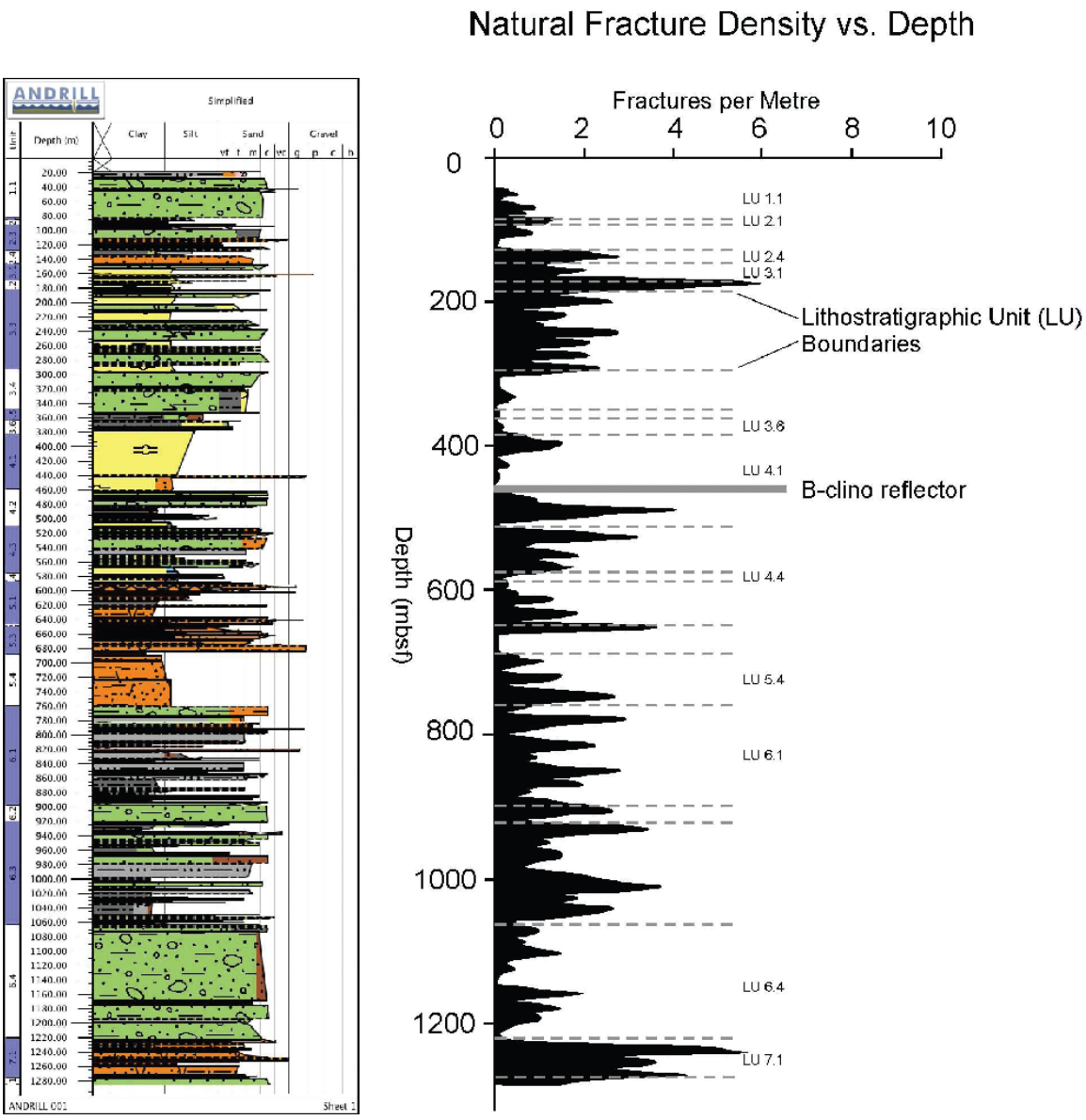

Figure 5 – This density plot represents the number of natural fractures in relation to depth (mbsf), lithostratigraphic subunit, and lithology.

From (Wilson et al., 2007)

van der Meer's Hypothesized Sequence of Glacial Microstructures

Place in Sequence	Feature
Upper pervasive deformation zone	Omnisepic fabric generally
	Discrete shears
	Type I pebbles (*in situ* with no internal fabric)
	Type II pebbles (*in situ* with internal fabric)
	Skelsepic fabric
Middle pervasive deformation zone	Lattisepic fabric generally
	Discrete shears
	Type I pebbles (*in situ* with no internal fabric)
	Pressure shadows
	Masepic fabric
Lower pervasive deformation zone	Skelsepic fabric generally
	Discrete shears
	Type I pebbles (*in situ* with no internal fabric)
	Type III pebbles (reworked)
	Kinking fabric
Upper brittle deformation zone	Discrete shears
	Type I pebbles (*in situ* with no internal fabric)
	Discretely sheared soft clasts
	Crushed grains
	Dewatering and escape structures (presumably involving downwards escape)
	Kinking fabric

Figure 6 – This chart displays microfabrics and microstructures that are commonly found within four zones which represent the proximity of a glacier to the underlying rock being deformed.

(from Evans, 1998)

METHODS

Observations of the samples were analyzed micro- and macroscopically. Core images of samples 152.12mbsf, 166.64mbsf, 167.60mbsf, 168.00mbsf, and 178.04mbsf were provided and interpreted with the use of Adobe Illustrator along with hand notes and sketches provided by Dr. Terry Wilson and her graduate students. Thin sections of all of the samples were analyzed using a petrographic microscope. Each slide was then scanned and deciphered using Adobe Illustrator in conjunction with the results found using microscopy.

OBSERVATIONS

I examined the microstructures and microfabrics in six thin sections that were obtained from the Andrill-1B core. The depths of these samples are: 152.12 mbsf, 166.64 mbsf, 167.60 mbsf, 168.00 mbsf, 178.04 mbsf, and 189.67 mbsf. The images below provide visual representations of the microfabrics and microstructures viewed within the thin sections.

152.12 mbsf – Mudstone with dispersed/common clasts

Core Image

This section of the core contains several large clasts that are subrounded to angular. The bedding is discontinuous, wavy, and parallel. There is a thick, dark, wavy vertical band that extends the length of the sampling area. In areas where the band overlies bedding, the bedding appears to become truncated by the band.

I was able to identify seven faults, five within the sampling area and two outside of the sampling area. Four of the faults within the sampling area produced offset of the band. Three of the four faults show reverse displacement and the fourth fault shows normal displacement. The fifth fault in the sampling area does not display noticeable offset within the sampling area, but I was able to trace the fault in the left, down core direction from the sampling area at which point I observed reverse displacement in a brown band. Below this fault, outside of the sampling area, is a different band with reverse displacement from another fault. The second fault outside of the sampling area has offset the bedding in the upper right corner of the core image. The bedding shows reverse displacement. In **Figure 8**, I have outlined the band and labeled the bedding, faults, and shear sense.

Thin Section

The thin section revealed a few of the large clasts to be of volcanic origin. These clasts are angular. The sample contains an abundance of opaques that are rounded to subangular and range in size from 0.05mm to 1.2mm under 100x magnification. Several of the clasts in this sample are partially to fully coated by fine grained sediment. The bedding consists of discontinuous, even and wavy, parallel laminae. The boundaries of the band were not as discernible as in the core image.

Several of the clasts exhibit σ-type microstructures. Due to the orientation and cut of the thin section, a few of the microstructures do not show shear sense.

I was only able to identify two of the five faults seen in the core. The offset of the band is very subtle and extremely difficult to see. I have outlined the band and labeled the bedding, faults, and shear sense in **Figure 9**.

166.64 mbsf – Diatomite

Core Image

The features in this image are extremely difficult to see due to the marks made by the

rock saw. However, I was able to identify two nearly parallel faults that have offset bedding. The bedding has been normally displaced by the fault on the right (**Figure 10**). Unfortunately, I am unable to determine the shear sense of the other fault.

Thin Section

Opaques are subangular to rounded and range in size from 0.05mm to 0.4mm under 100x magnification. The bedding is offset in three locations, each by a different fault. Two of the faults appear to be almost parallel; whereas the third fault is angled toward the other faults. All of the faults show normal displacement (**Figure 11**).

167.60 mbsf – Diatomite

Core Image

There are several large clasts in the image, but only a few within the sampling area. There is bedding both within and outside of the sampling area. There are several bands outside of the sampling area and one or two within the sampling area. I was able to identify twenty-seven faults from offset of the bedding and several of the bands. Fifteen of the faults extend either through or in to the sampling area and the other twelve faults are outside of the sampling area. Six of the faults in the sampling area show normal displacement. I was unable to identify the shear sense of the other nine faults. The faults outside of the sampling area all show normal displacement. I have labeled the bedding, faults, and shear sense in **Figure 12**.

Thin Section

There are few clasts (< 5%) present in this sample. Opaques are rounded to subangular and range in size from 0.05mm to 0.6mm under 100x magnification. Drag folds are present in some parts of the bedding. Also, drag folds can be seen in three of the bands, two of which form en echelon drag folds. Using the offset and drag folds of the bedding and bands, I was able to identify seventeen faults. Two of the faults show normal-sense displacement and I was unable to determine the shear sense of the other faults. There is a small section in the sample that appears to have crenulation. In **Figure 13**, the drag folds are outlined and the bedding, faults, and shear sense are labeled.

168.00 mbsf – Diatomite

Core Image

There are several large clasts in the image, but only a few in the sampling area. The bedding shows normal displacement in four locations. Also, there is noticeable offset in sediment throughout the image. I identified nine faults in the image, five are within the sampling area. Four of the faults in the sampling area show normal displacement. The other fault, which has been sheared three times, shows reverse displacement. The four faults outside of the sampling area all show normal displacement (**Figure 14**).

Thin Section

The bedding shows offset in four locations, all of which have normal displacement. The bedding, faults, and shear sense are labeled in **Figure 16**. Opaques are rounded to subangular and range in size from 0.05mm to 0.5mm under 100x magnification.

178.04 mbsf – Diatomite

Core Image

The bedding in this core image is located beneath two dark bands in the sampling area. I was able to identify five places that the bedding had been offset. There are also three bands in this image that display offset, two of the bands are inside the sampling area and the other band is outside of the sampling area.

The first band that displays offset is present both within and outside the sampling area. The band is dark gray-black in color and is located directly above the bedding. This band shows normal displacement in four locations. The second band is a greenish-gray color and is located beneath the left half of the dark gray-black band. This band shows reverse displacement. The band outside of the sampling area is dark gray in color and shows normal displacement. I have outlined the bands and labeled the bedding and faults in **Figure 16**.

Thin Section

The bedding and two bands inside the sampling area are both identifiable in the thin section. Unfortunately, most of the left half of the band above the bedding is missing. The band above the bedding does show normal displacement in three locations. Offset in the bedding is not as easy to discern compared to the core image. I have outlined the bands and labeled the bedding and faults in **Figure 17**. Opaques are rounded to subangular and range in size from 0.05mm to 0.5mm under 100x magnification.

189.67 mbsf – Mudstone with dispersed/common clasts

Thin Section

There was no core image available to accompany this thin section which prevented me from being able to identify the bedding. However, I was able to identify several opaques in the image with microstructures. Unfortunately, due to the orientation of the microstructures and the cut of the thin section, the sense of shear is unable to be determined. Opaques are rounded to subangular and range in size from 0.1mm to 1mm under 100x magnification.

I was also able to identify one in this thin section. The first fault runs through the middle of the core in the up and down core directions. Unfortunately, I was unable to determine the shear sense of this fault. The fault and microstructures are labeled in **Figure 18**.

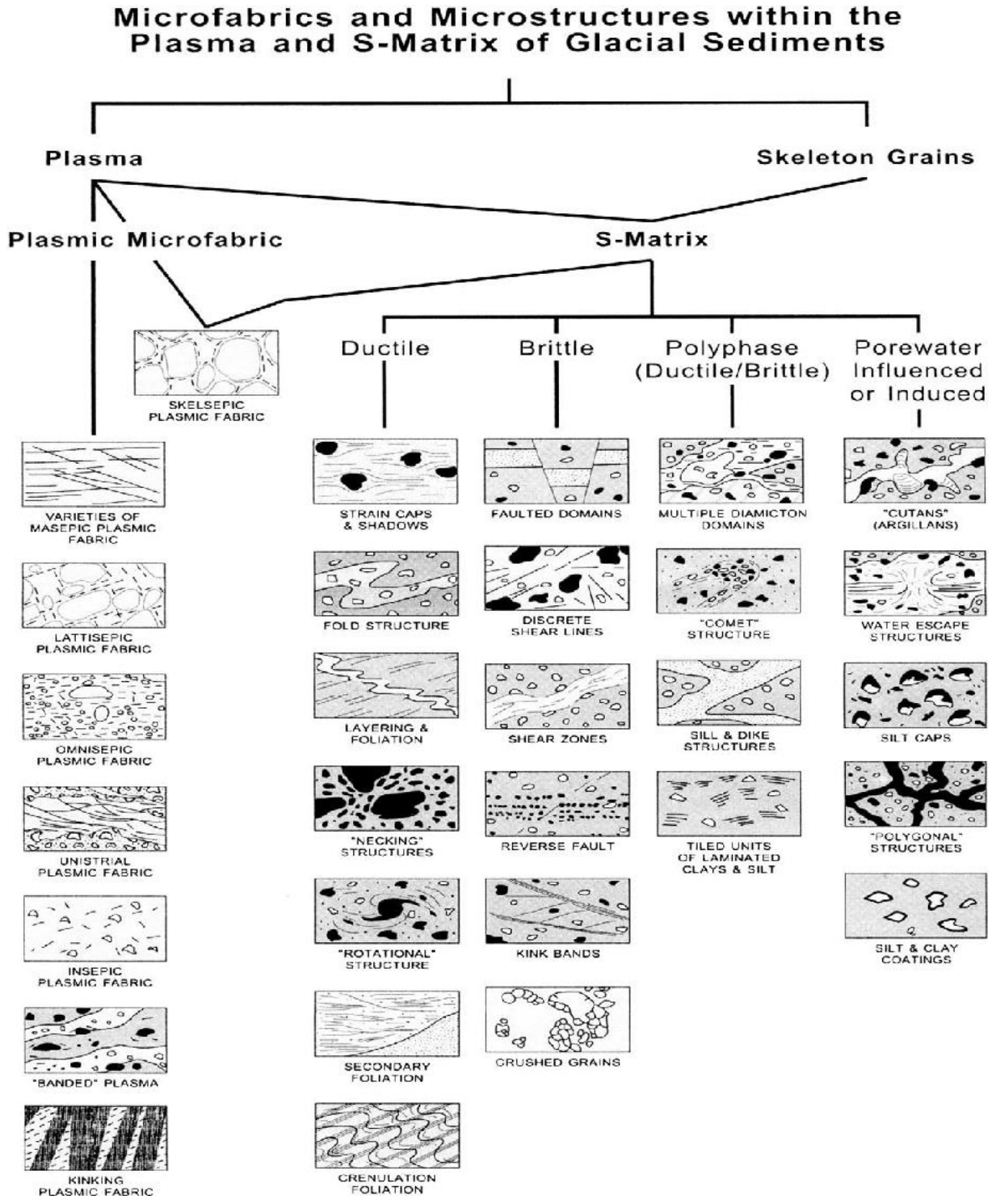

Figure 7 – The microfabrics and microstructures illustrated are categorized according to the form of deformation that has occurred.

From (van der Meer et al., 2003)

Discussion

Through the use of thin section and core analyses, I was able to identify fabrics and structures within the six samples. The micro- and macrostructures observed were used in determining the mechanism(s) of deformation for each sample.

Core Analysis

Core images were observed for samples: 152.12 mbsf, 166.64 mbsf, 167.60 mbsf, 168.00 mbsf, and 178.04 mbsf. Unfortunately, very few, if any, macrostructures were able to identified and, therefore, interpreted for each sample.

In sample 152.12mbsf, I identified a band that displayed offset in four areas. The offset was produced by reverse faults. This sample is within 5m of a GSE and displays brittle deformation through reverse faulting. This is consistent with the prediction that this sample could display glaciotectonic deformation.

Sample 166.64mbsf displayed marks along the surface left by the rock saw used on the core. Although the rock saw obscured most of the macrostructures from being identifiable, I was able to find offset of the bedding in six locations. Consequently, I was unable to determine the shear-sense of any of the faults.

The core image for sample 167.60mbsf displayed twenty-seven faults. Of the twenty-seven faults, I was able to identify sixteen normal faults and one reverse fault. The normal faults are consistent with the half-graben and expected conjugate faulting from tectonic deformation. The reverse fault is most likely the result of glaciotectonic deformation.

In the area of the core used to make thin section for sample 168.00mbsf, the bedding is normally offset in three locations. The normal faults are congruous with tectonic deformation.

The final core image analyzed from 178.04mbsf shows normal displacement of the bedding in three areas and a possible reverse displacement in one area. The presence of a reverse fault is inconsistent with the anticipated lack of glaciotectonism. The nearest GSE to the sample is nearly 15m above which may have resulted in deformation to the bedding in this sample. However, the normal faults are present as expected.

There was no available image to interpret from the core for sample 189.67mbsf.

Thin Section Analysis

In sample 152.12mbsf I was able to identify two of the four faults observed from the core image. Unfortunately, due to either the cut and/or lithologies found in the thin section, deciphering the remaining two faults or the shear-sense was not possible. However, it was possible to define the band seen in the core image and the bedding is finely laminated. A few grains display silt and/or clay coating which could be porewater induced or influenced.

Sample 166.64mbsf, displays offset in four locations. The bedding is offset by two faults, one with normal-sense and the other with reverse-sense. The remaining two faults offset a band; unfortunately, I was only able to identify the shear-sense of one of the faults, which is normal-sense displacement. The presence of faults is the result of brittle deformation. However, the normal faults are the result of the half-graben; whereas the reverse fault is most likely the result of glaciotectonism. The sample is 2.99m below a GSE and, therefore, is likely to undergo glacial deformation.

The bedding in sample 167.60mbsf is offset by nine faults and five microfaults. Also, the clays in the sample display offset by three additional faults. I was only able to identify the shear-sense of two of the faults due to the presence of a drag fold with normal displacement. The normal faults are the result of brittle deformation by tectonism. There is a shear zone that occurs within an area of clay which is, also, the result of brittle deformation; however, the presence of a shear zone may be indicative of glaciotectonism. Additionally, there is an area that displays crenulation which is the result of ductile deformation. Four of the grains in this sample have internal plasmic fabric. Two of the grains have omnisepic fabric while the other two have bimasepic fabric. According to van der Meer's classification, these are type II grains and may be the result of ductile deformation. However, the grains do not show any sign of alignment. The ductile deformation is most likely the result of glacial deformation which is congruous with the sample being 3.95m below a GSE.

In sample 168.00mbsf the bedding and a band have been offset in three locations. All three of the faults display normal displacement as the result of brittle deformation due to tectonism. The grains in this sample exhibit omnisepic, bimasepic, trimasepic, and quadmasepic internal plasmic fabrics. This sample, also, contains van der Meer's type II grains. Unfortunately, the grains in this sample do not show any sense of alignment. The presence of grains with internal plasmic fabrics could be the result of ductile deformation. The sample is 4.35m below a GSE which is consistent with the ductile deformation being a result of glaciotectonism.

Similarly to sample 152.12mbsf, due to either the cutting of the core or the lithologies present it was very difficult to identify many features in sample 178.04mbsf. However, I was able to identify two faults with normal displacement. These faults are the result of brittle deformation from tectonism. A few of the grains in the sample did contain bismasepic fabric and are, therefore, type II grains. The presence of internal plasmic fabric inside some of the grains suggests that the sample underwent ductile deformation. The grains in this sample showed no alignment. Consequently, this sample is 14.39m below a GSE which is inconsistent with only the samples that are within 10m of a GSE undergoing deformation.

Sample 189.67mbsf contains what appears to be a vein running in the up/down direction of the thin section. Unfortunately, there is no material inside of the vein which could be a result from the rock saw. The presence of a vein is the result of fracturing/faulting due to brittle deformation. I was unable to identify any faults within this sample. However, there are several grains that contain omnisepic and trimasepic internal fabric which is indicative of type II grains. The presence of type II grains suggests that ductile deformation occurred. Congruent with the grains seen in the other samples, there is no alignment. This sample occurs 6.68m below a GSE which is consistent with the possibility this sample underwent glaciotectonism.

Glacial and/or Tectonic Deformation

All of the samples observed displayed structures associated with brittle and ductile deformation Furthermore, all of the samples exhibit features identified by van der Meer as occurring in the upper pervasive zone. The presence of glacial deformation for all of the samples except 178.04mbsf, were consistent with samples undergoing deformation that are within 10m of a GSE.

The samples that contained normal faults and/or conjugate normal faults, were most likely the result of tectonic deformation due to the half-graben and Terror Rift. Samples 166.64mbsf, 167.60mbsf, 168.00mbsf, and 178.04mbsf all display brittle deformation through

normal faulting. Drag folds that display normal-sense displacement are also present in sample 167.60mbsf.

Several of the samples contain brittle and ductile deformation that could be the result of glaciotectonism. Reverse faults, which are believed by Wilson et al. to be associated with glacial deformation, are present in samples 152.12mbsf, 166.64mbsf, and 167.60mbsf (Wilson et al., 2008).

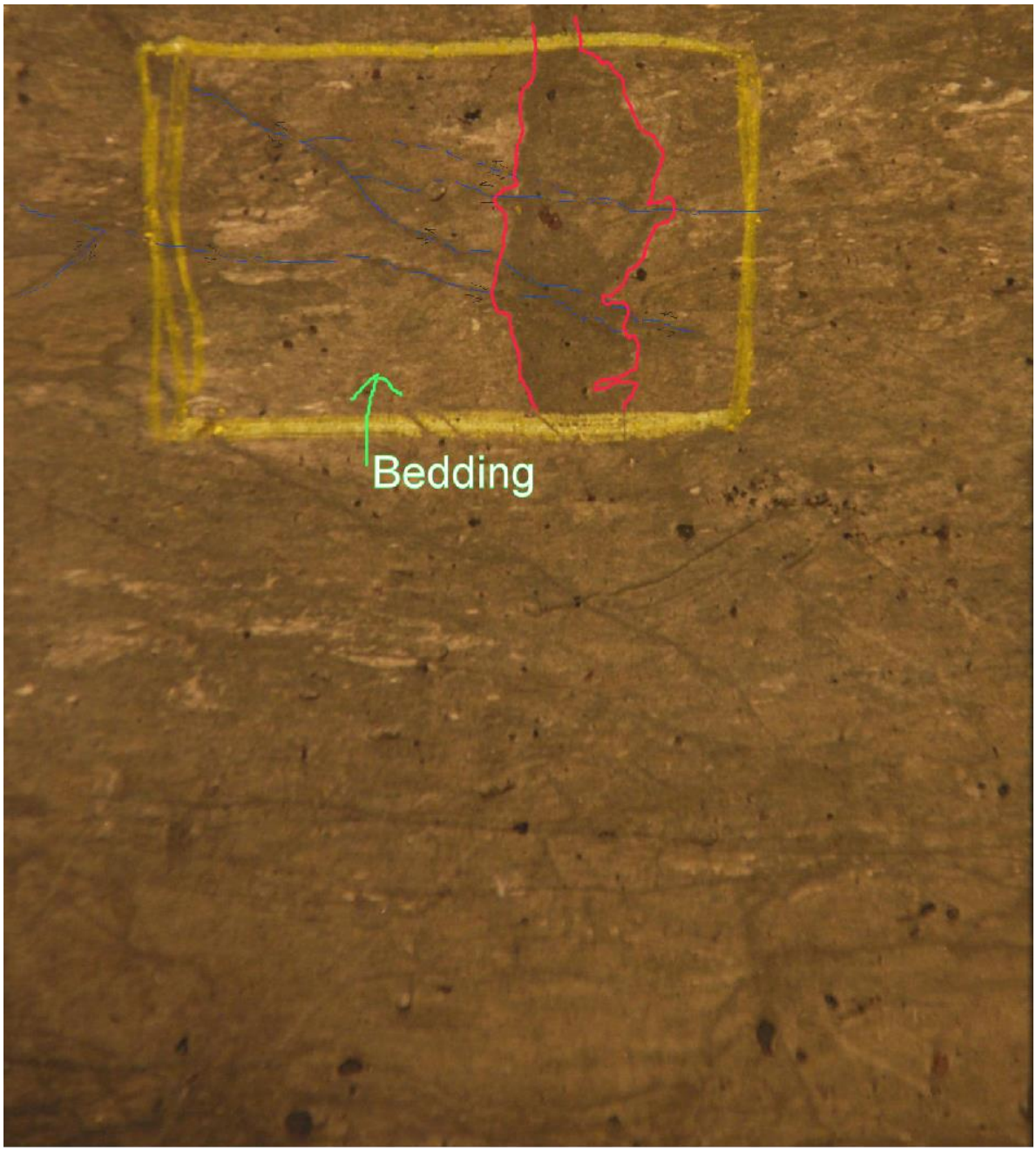

Figure 8 - Core Image 152.12mbsf

Figure 9 - Thin Section 152.12mbsf

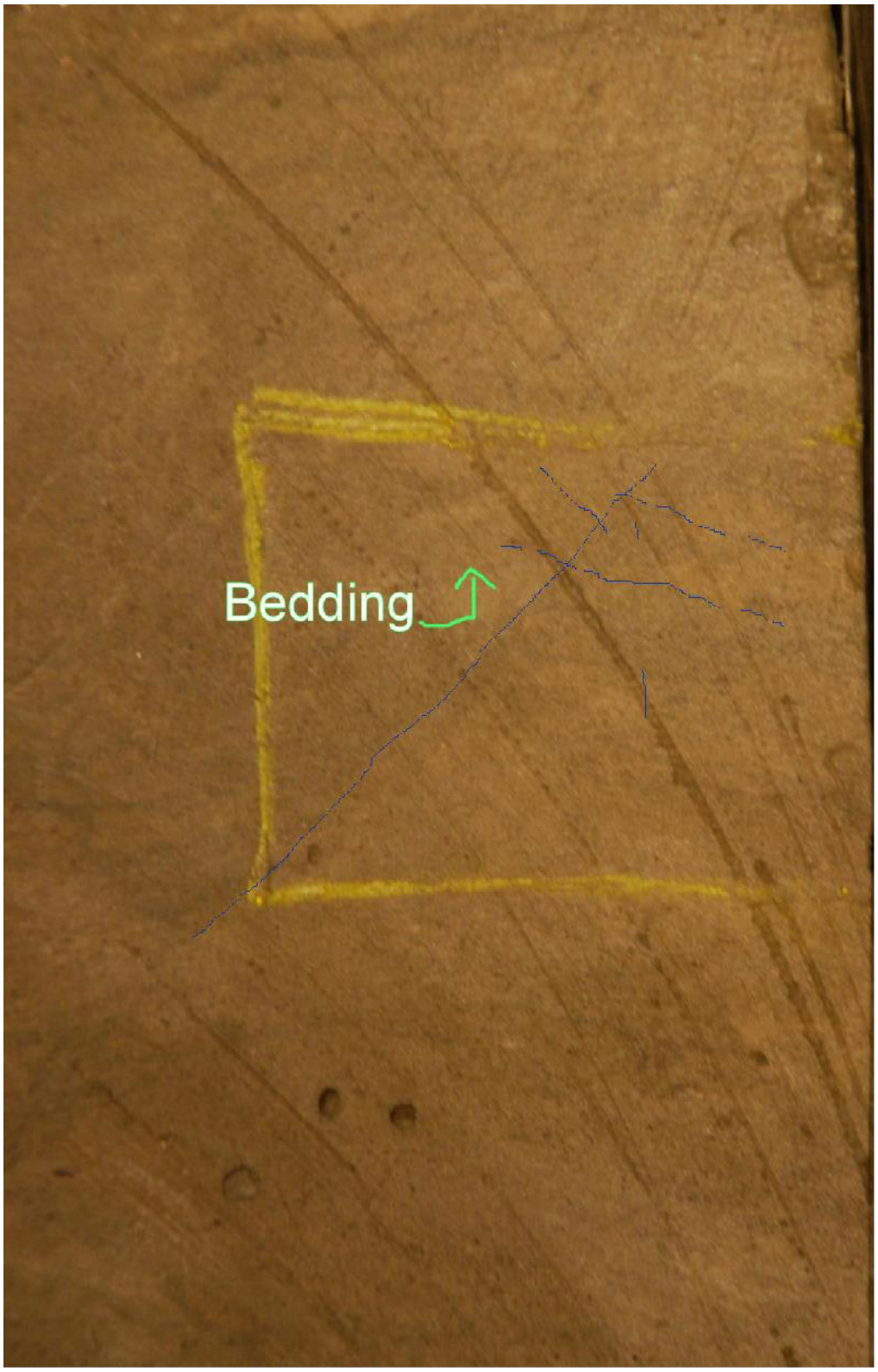

Figure 10 – Core Image 166.64mbsf

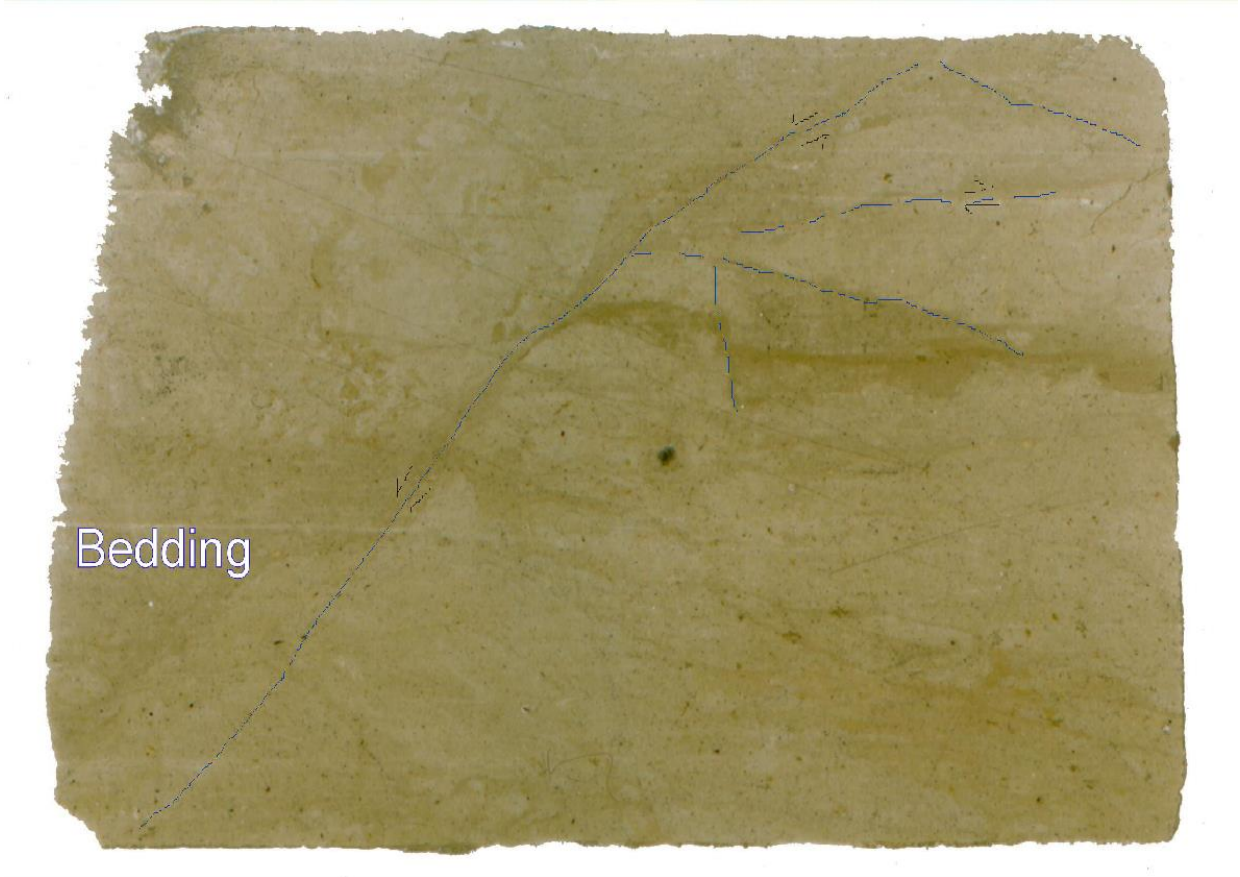

Figure 11 - Thin Section 166.64mbsf

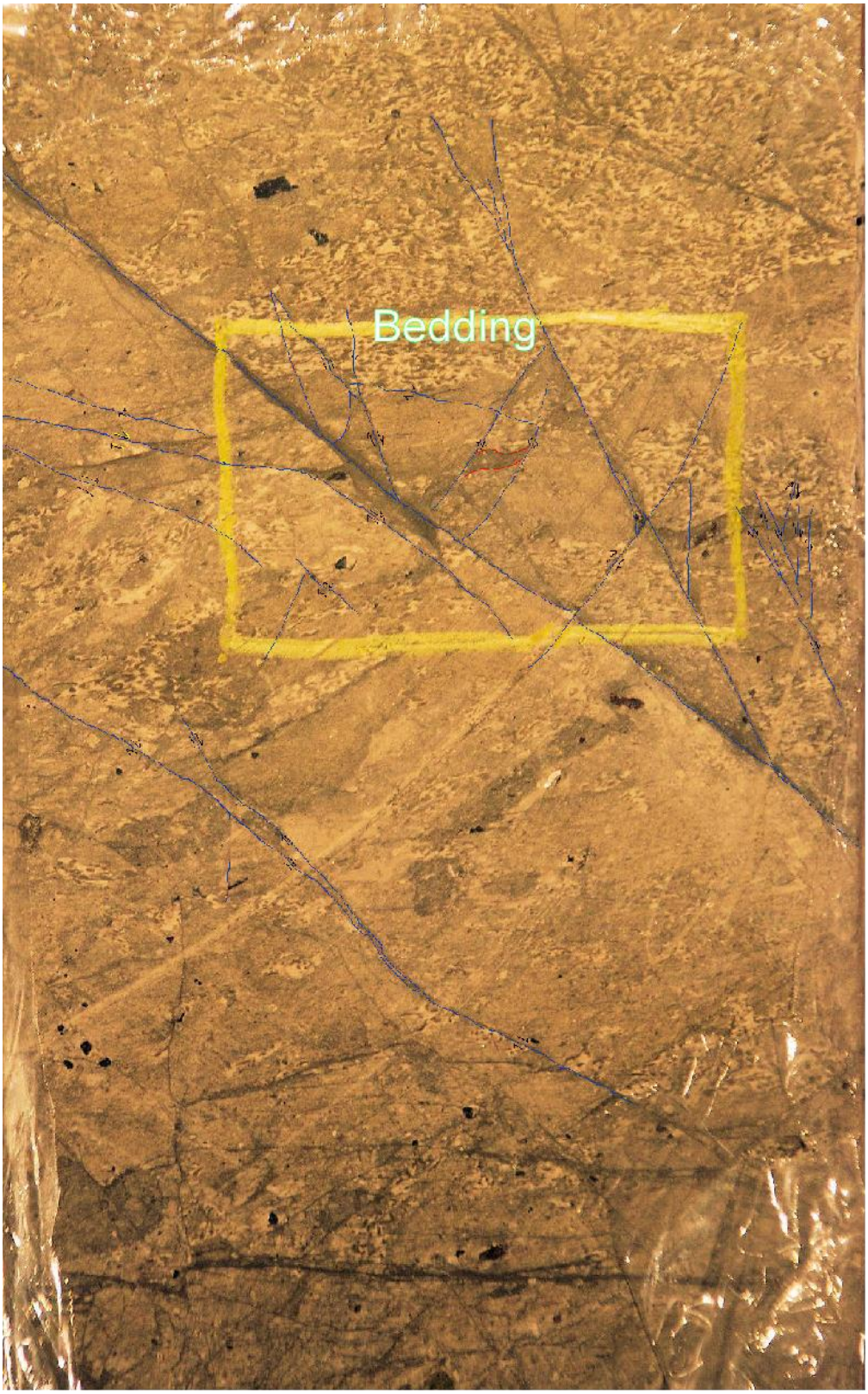

Figure 12 - Core Image 167.60mbsf

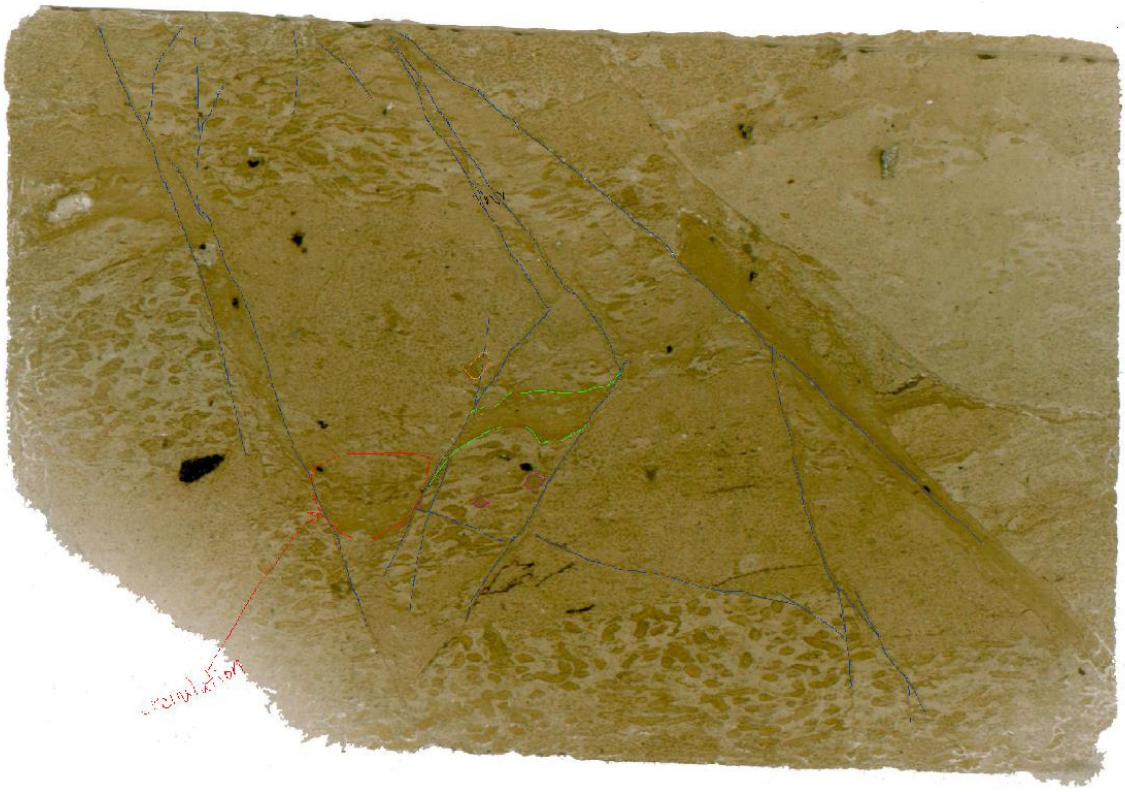

Figure 13 - Thin Section 167.60mbsf

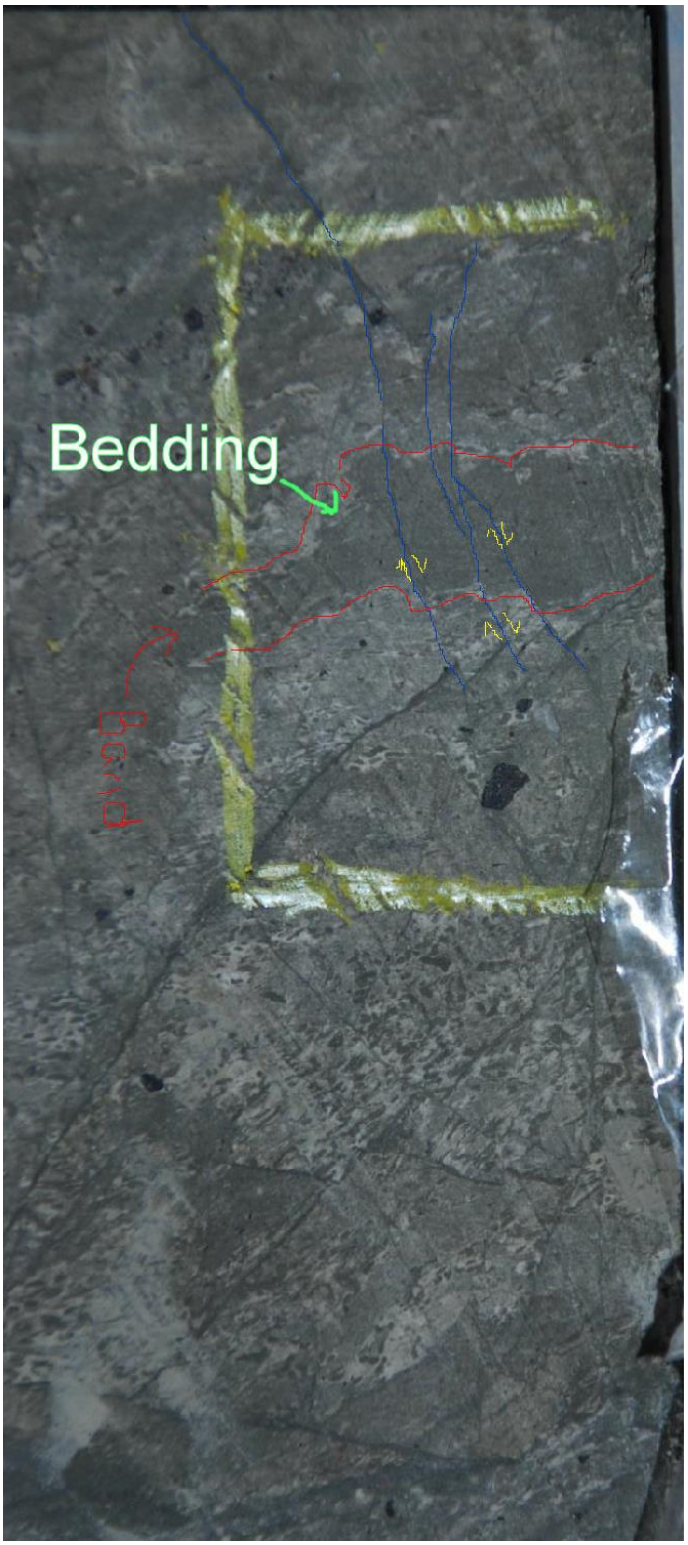

Figure 14 - Core Image 168.00mbsf

Figure 15 - Thin Section 168.00mbsf

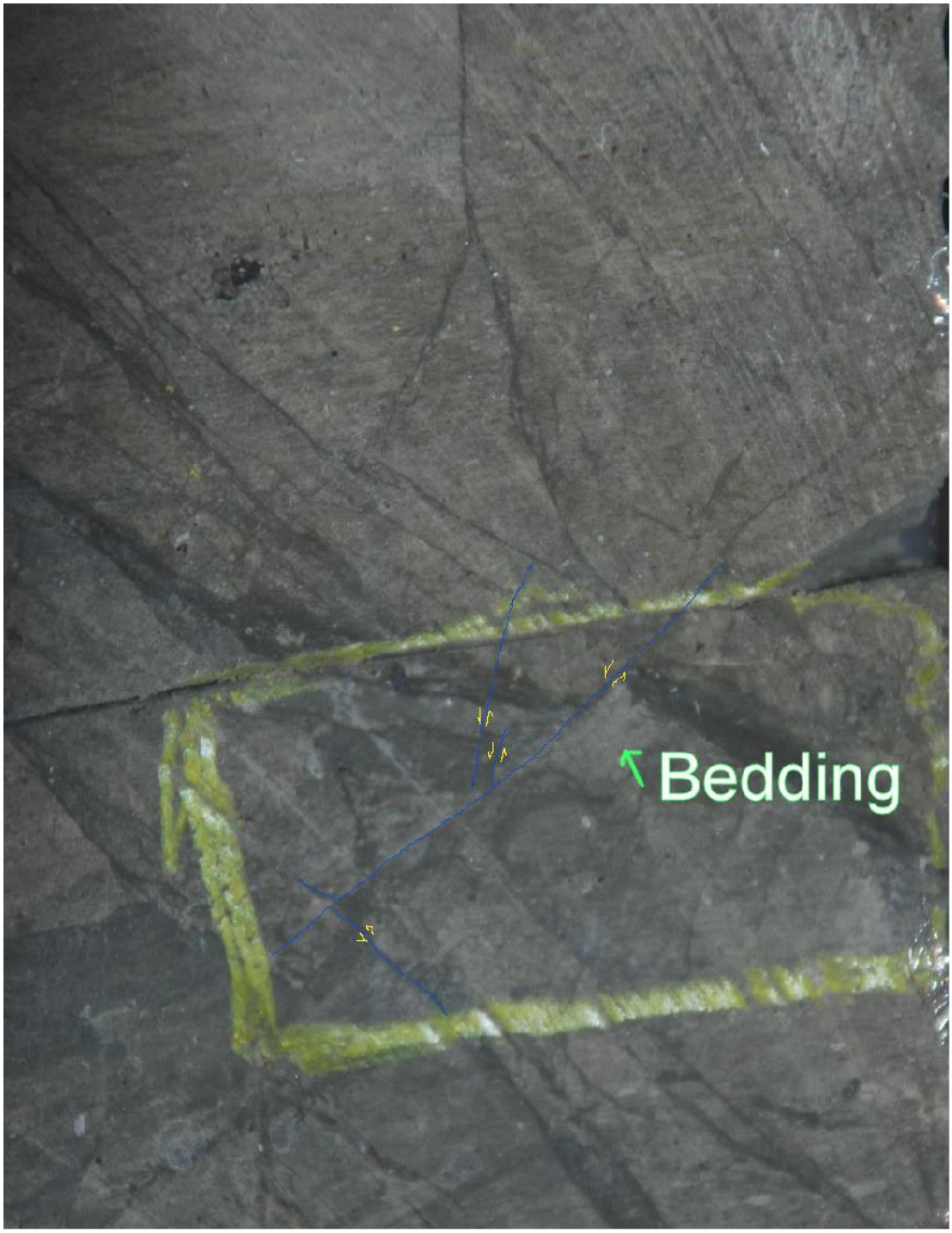

Figure 16 - Core Image 178.04mbsf

Figure 17 - Thin Section 178.04mbsf

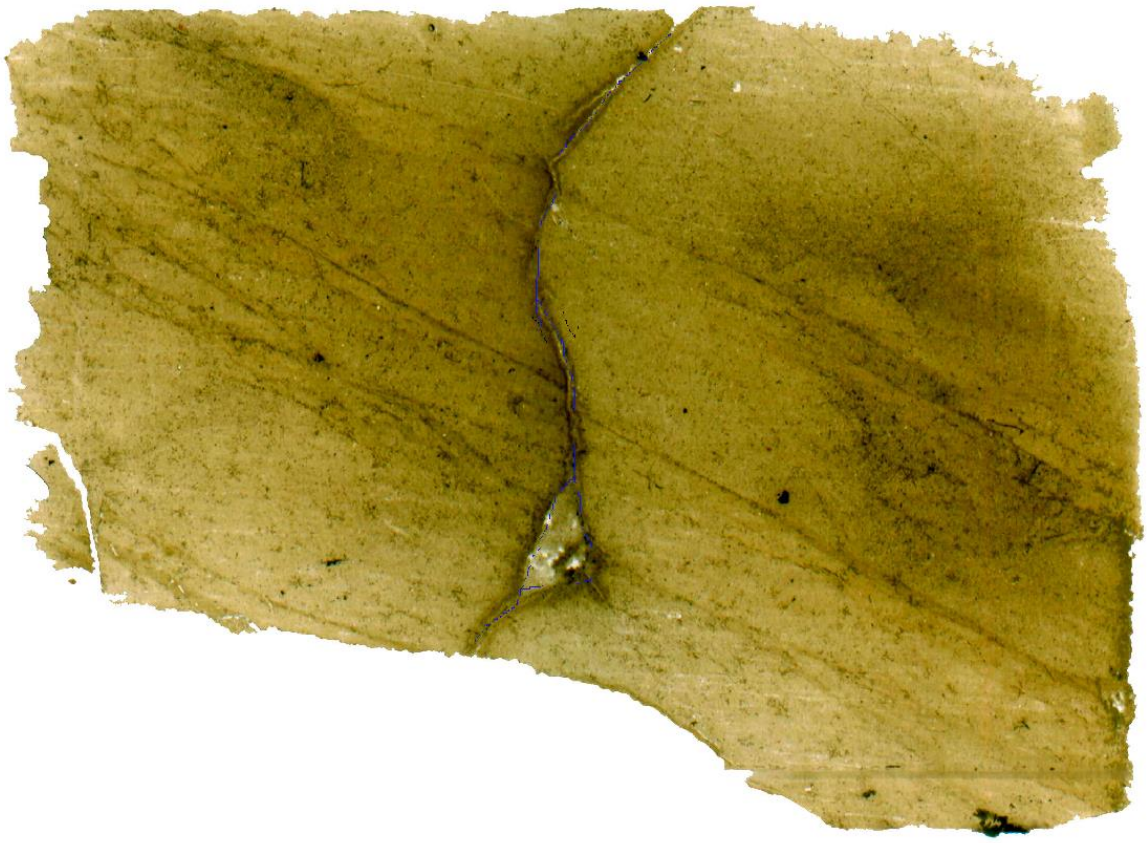

Figure 18 - Thin Section 189.67mbsf

CONCLUSIONS

The Victoria Land Basin has undergone many glacial-interglacial cycles which is evident through the core images and thin sections observed. The samples display three different glacial proximity settings upon deposition with four samples in a marine setting (166.64mbsf, 167.60mbsf, 168.00mbsf, and 178.04mbsf), one sample in a distal setting (152.12mbsf), and one sample in a setting with ice contact (189.67mbsf).

Evidence of brittle and/or ductile deformation is present in all of the samples based on features associated with having occurred in the upper pervasive zone as defined by van der Meer. Samples 152.12mbsf, 166.64mbsf, and 167.60mbsf exhibit reverse faulting consistent with observations made by Wilson et al. that evidence of glaciotectonism may be present within 10m of a glacial surface of erosion. As expected during times of marine settings, samples 166.64mbsf, 167.60mbsf, 168.00mbsf, and 178.04mbsf display evidence of normal and/or conjugate normal faults which is most likely the result of deformation due to the half-graben within the Victoria Land Basin and Terror Rift.

Due to damage to core samples and thin sections along with difficulties due to lithology of samples, shear sense was not able to be determined for all of the faults identified. However, for most of the samples evidence of glacial vs. tectonic deformation was able to be determined based on faults with identifiable shear sense. Consequently, with the distance between the samples used in this research, the anomaly of a reverse fault seen within sample 178.04mbsf is unable to be explained at this point in time.

RECOMMENDATIONS FOR FUTURE WORKS

Suggestions for future work would be to investigate samples closer to glacial surfaces of erosion to understand the deformation formed in glacial environments. Additionally, use of samples that are within closer proximity to one another may provide a more comprehensive understanding as to the underlying cause of anomalies, such as the deformation seen in 178.04mbsf. Furthermore, selection of samples with corresponding core images and thin sections will allow for more detailed analysis as well as a more comprehensive view of surrounding features and/or deformation

REFERENCES CITED

Aber, J.S., and Ber, A., 2007, Glaciotectonism: Amsterdam, Elsevier, Developments in Quaternary Science, v. 6, 246 p.

Evans, A., 1998, The Causes and Implications of Microstructures in Glacial Sediments [Ph. D. Thesis]: Leeds, University of Leeds, 281 p.

Krissek L., Browne G., Carter L., Cowan E., Dunbar G., McKay R., Naish T., Powell R., Reed J., Wilch T., and ANDRILL-MIS Science Team, 2007, Sedimentology and Stratigraphy of the AND-1B Core, ANDRILL McMurdo Ice Shelf Project, Antarctica: Terra Antarctica, v. 14, p. 185-222.

McKay, R., Browne G., Carter L., Cowan E., Dunbar G., Krissek L., Naish T., Powell R., Reed J., Talarico F., and Wilch T., 2009, The stratigraphic signature of the late Cenozoic Antarctic Ice Sheets in the Ross Embayment: Geological Society of America Bulletin, v. 121, p. 1537-1561.

Menzies, J., 2000, Micromorphological analyses of microfabrics and microstructures indicative of deformation processes in glacial sediments: Geological Society of America Special Papers, v. 176, p. 245-257.

Naish T., Powell R., Levy R., and ANDRILL-MIS Science Team, 2007a, Background to the ANDRILL McMurdo Ice Shelf Project (Antarctica) and Initial Science Volume: Terra Antarctica, v.14, p.121-130.

Naish T., Powell R., Levy R., Henrys S., Krissek L., Niessen F., Pompilio M., Scherer R., Wilson G., and ANDRILL-MIS Science Team, 2007b, Synthesis of the Initial Scientific Results of the MIS Project (AND–1B Core), Victoria Land Basin, Antarctica: Terra Antarctica, v. 14, p. 317-327.

van der Meer J.J.M., Menzies J., and Rose J., 2003, Subglacial till: the deforming glacial bed: Quaternary Science Reviews, v. 22, p. 1659-1685, doi:10.1016/S0277-3791(03)00141-0.

van der Pluijm B.A., and Marshak S., 2004, Earth Structure, ed. 2: New York, W.W. Norton and Company, 656 p.

Wilson T.J., Paulsen T.S., Millan C., Läuefer A., McKay R., and ANDRILL MIS Science Team, 2008, Brittle fractures in AND-1B core, McMurdo Ice Shelf, Antarctica: A record of Neogene rifting or glaciotectonic deformation? Eos Trans. AGU, 89(53), Fall Meet. Suppl., Abstract C33A-05.

Wilson T., Paulsen T., Läufer A.L., and Millan C., 2007, Fracture Logging of the AND-1B Core, ANDRILL McMurdo Ice Shelf Project, Antarctica: Terra Antarctica, v. 14, p. 175-184.

Zaniewski K., and van der Meer J.J.M., 2005, Quantification of plasmic fabric through image analysis: Catena, v.63, p.109-127, doi:10.1016/j.catena.2005.07.001.

GLOSSARY

Adherent Matrix – Microstructure comprising of a grain that has an attached matrix layer on one or more edges. The matrix layer is exotic to the surrounding matrix.

Argillans – "Accumulation of clay particles within voids or other separations within the plasma" (Menzies, 2000).

Argillasepic Fabric – "A form of asepic plasmic fabric. Matrix consists of mostly clay sized material" (Zaniewski and van der Meer, 2005).

Asepic Fabric – (1) "Very few or no anisotropic plasma domains present" (Zaniewski and van der Meer, 2005). (2) Fabric with no apparent evidence of structural deformation/ translation.

Bimasepic Fabric – (1) Long, straight oriented domains in two directions. (2) Parallel orientations of fine (clay) particles in two directions.

Clino-bimasepic Fabric – A type of masepic fabric that has a conjugate pattern with a dihedral angle of ~ 45 - 60°.

Crystic-plasma Appearance – An intertextic fabric with common crystallaria that are present locally.

Cutan – "An accumulation of material on or against structural elements, walls, or pores, etc. in soils or sediments; can be the result of illuviation of crystallization" (Zaniewski and van der Meer, 2005).

Diamictite – (Lithified diamicton) A poorly or non-sorted conglomerate or breccia with a wide range of clasts, up to 25% of them gravel sized (greater than 2mm). Diamictites are composed of coarse, angular to well-rounded sedimentary clastic fragments, or other type of fragments (igneous and metamorphic rocks) supported by a typically argillaceous (clay sized) matrix.

Diamicton – (also known as diamict) – (Unlithified) A very poorly sorted sediment. Large sedimentary grains gravel size and larger (≥ 2mm) are set in a matrix or fine grains.

Diatomite – "Biosiliceous-bearing mudstone" (Naish et al., 2007b).

Discrete Shear – See Unistrial Fabric

Galaxy Structure – See Milky Way Structure

Hemipelagic – (1) Deep-sea sediment in which more than 25% of the fraction coarser than 5 microns is terrigenous, volcanogenic, and/or neritic origin. Such deposits usually accumulate near the continental margin. (2) Of the biogeographic environment of the Hemipelagic region with both neritic and pelagic qualities. (3) The region of the ocean extending from the edge of a shelf to the pelagic environment; roughly corresponds to the bathyal zone, in which the bottom is

660 to 3300 feet (200 to 1000 meters) below the surface. (4) Of or relating to, or comprising deposits or sediments containing the remains of pelagic organisms and material washed down from land.

Insepic Fabric – “Small plasmic fabric domains lacking preferred orientation” (Zaniewski and van der Meer, 2005).

Kink Bands – “Microscopic orientation of grains of any size such that the fabric sharply undulates. Usually associated with shear fabrics. Kinking usually undulates parallel to the direction of a nearby shear zone” (Evans, 1998).

Lattisepic Fabric – This consists of two sets of thin, linear areas, each with a single, length-parallel, internal orientation, arranged at around 90° to each other, though the term is also used to describe a more pervasive mix of grains in two directions. Short oriented domains in two perpendicular directions.

Masepic Fabric – There is only one set of bands, all pointing in the same direction, and each with a single, length-parallel, internal fabric.

Micromorphology – Microscopic examination of the composition and constituent structural elements of lithified and unlithified earth materials.

Milky Way Structure – (Also known as a Galaxy Structure.) This structure is due to rotation which causes the small grains to adopt a position of least resistance parallel to the larger grains.

Multisepic Fabric – Three or more preferred modes or orientation are identified.

Omnisepic Fabric – (1) In glaciology, a single orientation in horizontal fabrics. (2) All fine material is re-oriented in one or more distinct directions.

Plasmic Fabric – (1) Distribution and orientation of clay particles in the sediment matrix. (2) The arrangement of plasma, skeleton grains, and associated simple packing voids. (3) Arrangement of birefringent plasma domains. Plasmic fabric depends on the optical characteristics of plasma particles and on their arrangement in relation to each other.

Rotation – “The pivoting of a body around a fixed axis” (van der Pluijm and Marshak, 2004).

Sepic Plasmic Fabric – Have recognizable anisotropic domains with various patterns of preferred orientation.

Silasepic Fabric – “A form of asepic plasmic fabric. Plasma consists of mostly silt-sized material” (Zaniewski and van der Meer, 2005).

Skelsepic Fabric – The alignment of particles parallel to the sides of large grains. The pressures due to rotational movement result in skelsepic plasmic fabric.

Strain – “A distortion of change in shape of a body” (van der Pluijm and Marshak, 2004).

Subadjacent – Situated beneath something.

Subglacial – Situated or occurring underneath a glacier or ice sheet.

Translation – “A change in the position of a body” (van der Pluijm and Marshak, 2004).

Unistrial Fabric – (Also known as discrete shears) (1) This type of fabric has only been observed when the till is clayey. Discrete shears appear as bundles of very fine, parallel discrete shears. The discrete shears show a strong orientation in two directions, with little cross cutting. In more clayey zones, the discrete shears are associated with a well-developed skel-lattisepic or even omnisepic (= all plasma re-oriented) plasmic fabric. (2) Unistrial plasmic fabric can be defined as a form of Masepic plasmic fabric. Unistrial domains are long and narrow streaks of birefringent plasma. Their diagnostic definition is set by the length/width ratio of 20:1. The ratio is a tentative value based on visual observations of unistrial domains in glacial sediments. (3) Discrete, thin, continuous lines of oriented birefringent clay plasma. (4) Anisotropic clay (plasma) with sharp birefringence bands in one direction (Menzies, 2000).